Design, Implementation, and Performance Evaluation of an IoT-Based Body Mass Index (BMI) Machine

Omolola, S. A, Olowofela, S. S, Mathew, T. O*

Department of Electrical and Electronic Engineering, Federal Polytechnic, Ilaro, Ogun State, Nigeria

***Corresponding author**

DOI: https://doi.org/10.47772/IJRISS.2026.100600084

Received: 27 May 2026; Accepted: 01 June 2026; Published: 17 June 2026

ABSTRACT

Obesity is the leading cause of cardiovascular death in developed and developing countries, the Conventional health monitoring relies on individual, manual assessments of weight and height, which frequently result in human error in Body Mass Index and logging delays. However, there is a need for the design and Implementation an accurate IoT-Based Body Mass Index (BMI) Machine.

The design, Implementation, and Performance Evaluation of an IoT-Based Body Mass Index (BMI) Machine based on the Internet of Things (IoT) are presented in this study. The designed system incorporates a load cell with a HX711 instrumentation amplifier for weight acquisition and an ultrasonic sensor (HC-SR04) for height measurement. After processing the physical inputs, an MCU ESP8266 microcontroller determines the user's BMI and categorizes their health status in accordance with World Health Organization (WHO) guidelines. For real-time mobile application tracking, data is shown locally on a 20x4 LCD screen and quickly transferred via Wi-Fi to a cloud database (Firebase). When compared to calibrated manual equipment, experimental validation on 55 test subjects showed great systemic accuracy with modest mean error rates of 0.64% for height and 1.50% for weight. This intelligent provides a medical dependability.

INTRODUCTION

The term "globesity" describes the global obesity and overweight epidemic. In both developed and developing countries, it is a serious public health concern. According to a recent WHO study from (2021), about one in eight young people in Nigeria were overweight or obese. Overweight and obesity accounted for 15–30% of coronary heart disease mortality and 65–75% of new occurrences of type-2 diabetes mellitus. Overweight and obesity result from the body storing extra energy as fat over time (Hidayat and Fajrianti, 2020). The body mass index (BMI) of an individual is calculated by dividing their weight in kilograms by the square of their height in meters. A person's BMI is a good way to determine if they are overweight or underweight. It is determined by dividing the weight of the body in kilograms by the square of height in meters. That is:

$$\text{BMI} = \frac{\text{Weight (kg)}}{\text{Height (m)}^2}$$

Another definition of BMI is the percentage of body weight that is fat (Krisnadi, T., and Ridwanto, M. 2021). It is frequently used as an indicator of obesity, which is an effort to measure an individual's tissue mass (muscle, fat, and bone) and classify them as underweight, normal, overweight, or obese depending on the result. Previous methods for identifying overweight and obesity include skin-fold thicknesses, bioelectrical impedance (Fadil, A., & Thamrin, M. 2020), underwater weighing, dual energy x-ray absorptiometry, waist circumference (WC), and waist-hip ratio (WHR). In a similar vein, the World Health Organization (WHO 2025) offers broad cutoff lines that allow BMI to categorize people into four main groups. Obese (≥ 30 kg/m2), overweight (25-29.9 kg/m2), underweight (< 18.5 kg/m2), and normal (18.5-24.9 kg/m2). The BMI-based categories of adult overweight and obesity in Table 1 demonstrate the many forms of obesity and their corresponding morbidity [8]. Although the methods for calculating BMI are the same for adults and children, the interpretation of the results varies. BMI ratings for adults are independent of sex and age. Because body fat differs by sex and fluctuates with age, BMI is interpreted in relation to a child's age and sex for children and adolescents between the ages of

2 and 20. Underweight, healthy weight, overweight, and obesity in children are categorized using age and sex-specific percentiles. An individual's BMI-for-age shows the related position of the child's BMI value among children of the same sex and age.

A wall-mounted stadiometer is used in typical clinical workflows to measure height, and normal spring or digital bathroom scales are used to measure weight. After manually recording these numbers, a medical expert calculates the final index. This fragmented technique fails to log data for progressive health analytics, takes a long time, and is prone to computation errors.

The development of the Internet of Things (IoT) offers a practical solution to automate the gathering of clinical data. A smart BMI can rapidly calculate a user's parameters and sync the previous data to cloud platforms by combining contemporary sensors with a Wi-Fi-enabled microprocessor. In order to provide remote and instantaneous patient diagnostics, this study describes the hardware architecture, firmware logic, cloud integration, and calibration performance of an automated IoT BMI device.

LITERATURE REVIEW

Faradisa et al. (2022) expanded upon hardware-driven automated calculations by targeting the analytical limitations of standard BMI equations, which fail to separate fat accumulation from lean muscle tissue development. To establish a more holistic health metric, they integrated a Mamdani-type fuzzy logic algorithm (Min-Max rule structure) to continuously map raw physiological sensor feeds into distinct nutritional bands (e.g., very thin, thin, normal, heavy, and obese). Furthermore, they combined the calculated BMI and user demographics using a predictive formula from the *British Journal of Nutrition* to calculate overall body fat percentage. Utilizing an Internet of Things (IoT) model driven by an Arduino Mega 2560 and a NodeMCU ESP8266 Wi-Fi transceiver, the design enabled safe, real-time wireless storage and synchronization with an external dashboard. Their output classifications matched internal MATLAB computational frameworks and manual validation baselines exactly.

While automated diagnostic platforms support preventative personal care, exact mathematical guidelines are equally critical within clinical environments—particularly regarding regional pediatric anesthesia. Caudal epidural analgesia requires balancing minimal local anesthetic footprints against the danger of unintended high-level neuraxial block spreads.

Kaushal et al. (2020) conducted a double-blind, randomized controlled trial comprising 75 children undergoing infra-umbilical operations to analyze the performance differences between dosing models. The trial compared a spinal column height-based modified Spiegel formula against two conventional weight-based metrics: the Takasaki and Armitage formulae.

A primary requirement of an automated BMI platform is the hands-free extraction of human height. A shared technical strategy among the evaluated instrumentation layouts is the utilization of time-of-flight acoustic wave propagation. Akpan et al. (2019) and Olawuni et al. (2022) integrated the HC-SR04 ultrasonic transducer module into their physical designs. This sensor works by emitting a high-frequency ultrasonic burst which reflects off the crown of the subject's head, enabling the core microprocessor to determine absolute distance by evaluating the total duration of the returning echo pulse.

Isola et al. (2018) employed a similar acoustic topology using the proprietary Parallax PIN Gm ultrasonic distance sensor. These automated acoustic methods present a substantial advantage over historical height sensing alternatives, such as Light-Dependent Resistors (LDRs), which exhibit low resolution and high operational inaccuracy due to ambient lux fluctuations

To acquire body weight dynamically, modern electronic layouts move away from historical spring-loaded analog scales in favor of strain-gauge load cells structured to capitalize on Hooke's Law. Isola et al. (2018) and Olawuni et al. (2022) utilized localized structural frameworks featuring integrated load cells that monitor resistance fluctuations caused by mechanical stress when a patient stands on the scale

Akpan et al. (2019) refined this transducer framework by integrating an MHT1 compression button force load cell configured into a traditional four-element Wheatstone bridge circuit. Because the physical micro-strain changes on foil-type strain gauges only yield minute differential changes in output millivolts, these configurations require specialized signal conditioning. Consequently, the engineering designs incorporate high-precision HX711 analog-to-digital converter and amplifier modules to clean and boost the sensor signals before routing them to the primary processing boards

Gizduino ATMEGA328 Ecosystem: Olawuni et al. (2022) integrated a Gizduino ATMEGA328 processing architecture to govern localized hardware interactions. This framework paired with an advanced software pipeline consisting of Microsoft Visual Studio (NET) and SQL Server Management Studio to create an external, persistent relational database. This configuration ensures patient files and historical BMI records can be securely queried over time for systematic diagnostic follow-ups

Arduino Mega 2560 Platform: Akpan et al. (2019) built their system around an Internet-ready Arduino Mega 2560 embedded platform. This processing core manages complex data pathways, coordinates visual outputs on an intelligent liquid crystal display (LCD), and supports standalone operation. To ensure outdoor utility in rural or off-grid areas, this system features a two-way automatic backup power supply module driven by a 12V Lithium-Polymer (Li-Po) rechargeable battery network.

Localized C-Program Microcontrollers: Isola et al. (2018) engineered a streamlined system governed by a microcontroller programmed entirely via embedded C-code. This system prioritizes low-cost manufacturing and rapid localized computations, routing raw mathematical outputs directly to an onboard alphanumeric LCD screen.

METHODOLOGY AND SYSTEM ARCHITECTURE

The Hardware Data Acquisition Layer, Processing and Control Layer, and Cloud Communication Layer are the three basic layers that make up the system architecture. The block diagram for the IoT-based BMI system seen in figure 1 consist the following hardware, ESP8266 micro-controller, weight sensor, Laser distance sensor (Tof400), Telegrams, LCD display, WIFI Module, Battery management system (BMS) and LiPO battery. The circuit diagram for the IoT-based BMI is as shown in figure 2.

The HX711 load cell amplifier is connected to the ESP8266 by wiring its DT pin to GPIO12 (D6) and its SCK pin to GPIO14 (D5), while the load cell itself is connected to the HX711 module using its red, black, white, and green wires according to the manufacturer's colour code. The VL53L1X Time of Flight (ToF) sensor communicates via I2C, so its SDA pin is connected to GPIO4 (D2) of the ESP8266, its SCL pin to GPIO5 (D1), and its VCC and GND pins to 3.3V and ground respectively. The 16×2 I2C LCD also uses the I2C bus, sharing the same SDA (GPIO4/D2) and SCL (GPIO5/D1) lines as the ToF sensor, while its VCC and GND are connected to 5V and ground. The push button is wired with one leg to GPIO15 (D7) and the other leg to ground, using the ESP8266's internal pull-up resistor so that pressing the button pulls the pin LOW. The ESP8266 board itself is powered through the Vin pin (5V) and ground, and it provides 3.3V logic levels for the ToF sensor as well as 5V for the LCD and HX711. The WiFi and Telegram connections are established through the ESP8266's on board wireless module, which communicates with the cloud no physical wiring is needed for internet connectivity. Finally, all components share a common ground (GND) to ensure stable signal reference. The Figure 3 Is the construction of IoT-based BMI Machine.

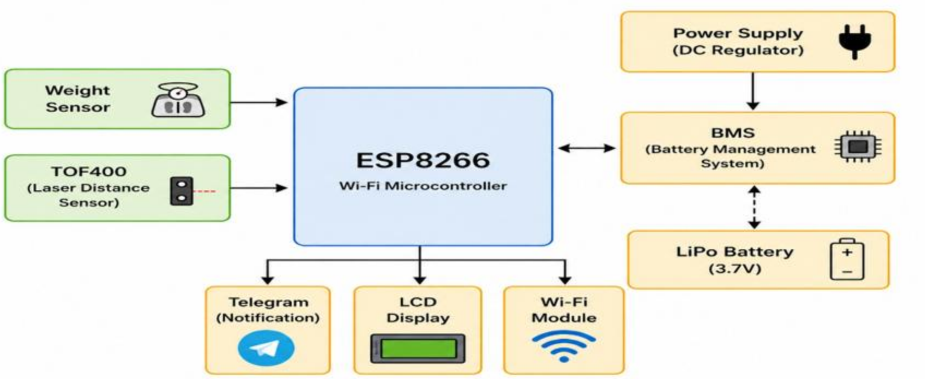

Figure 1: Block diagram of IoT-based BMI system

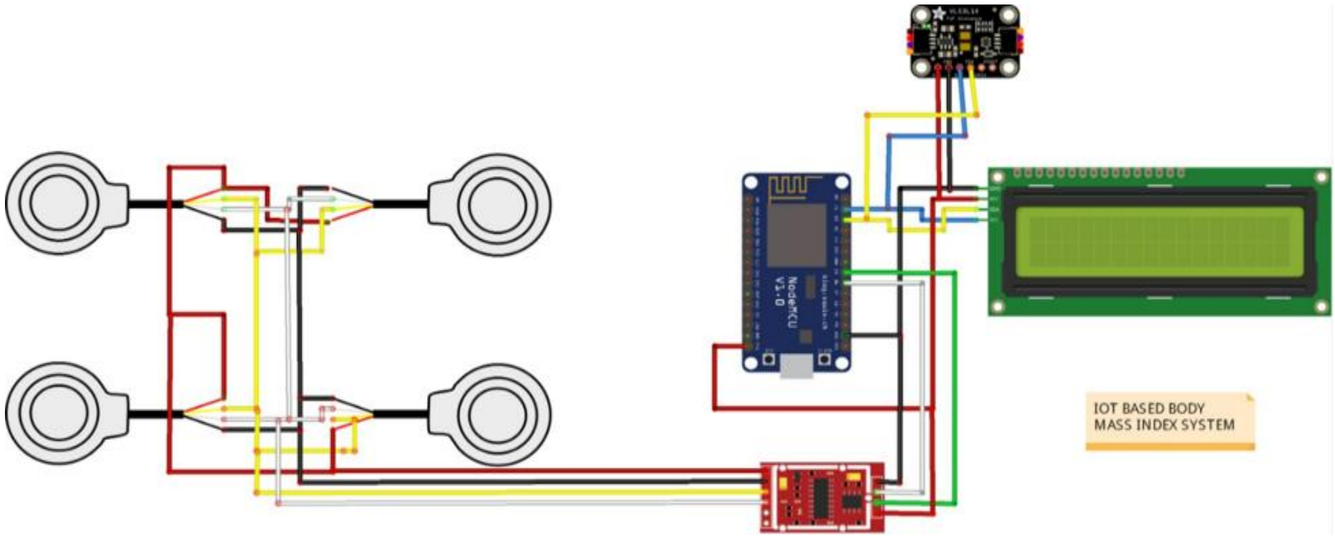

Figure 2: IoT-based BMI Circuit diagram

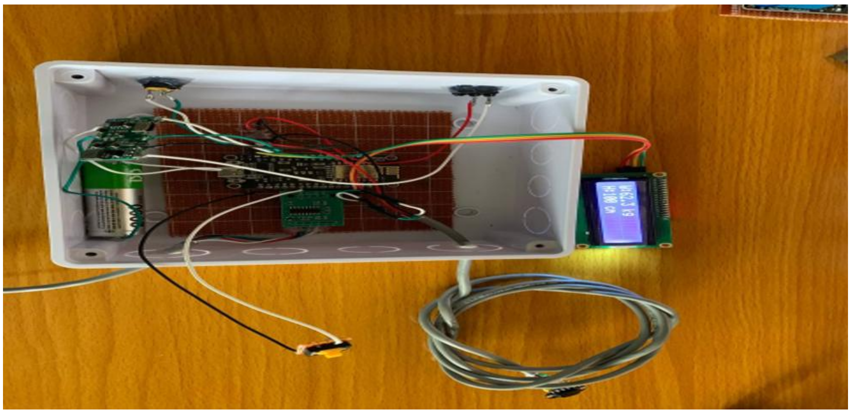

Figure 3. IoT-based BMI construction

RESULTS AND DISCUSSION

The load cells in the Figure 4. coupled with the laser distance sensor send the analog data (weight and height) to the microcontroller, and the program on the microcontroller sends the received data from the analog to digital to the display unit with the help of a digital signal converter. The data obtained is then processed, and the Arduino Uno microcontroller then uses these values to calculate the BMI. Figure 5 display the status of the user on the LCD screen based on the value of the calculated BMI and as well send the result through the internet to the data base of the patient as shown in figure 6.

Figure 4. Measurement posture sample

Figure 5. Picture of the LCD displaying the status of an individual during testing.

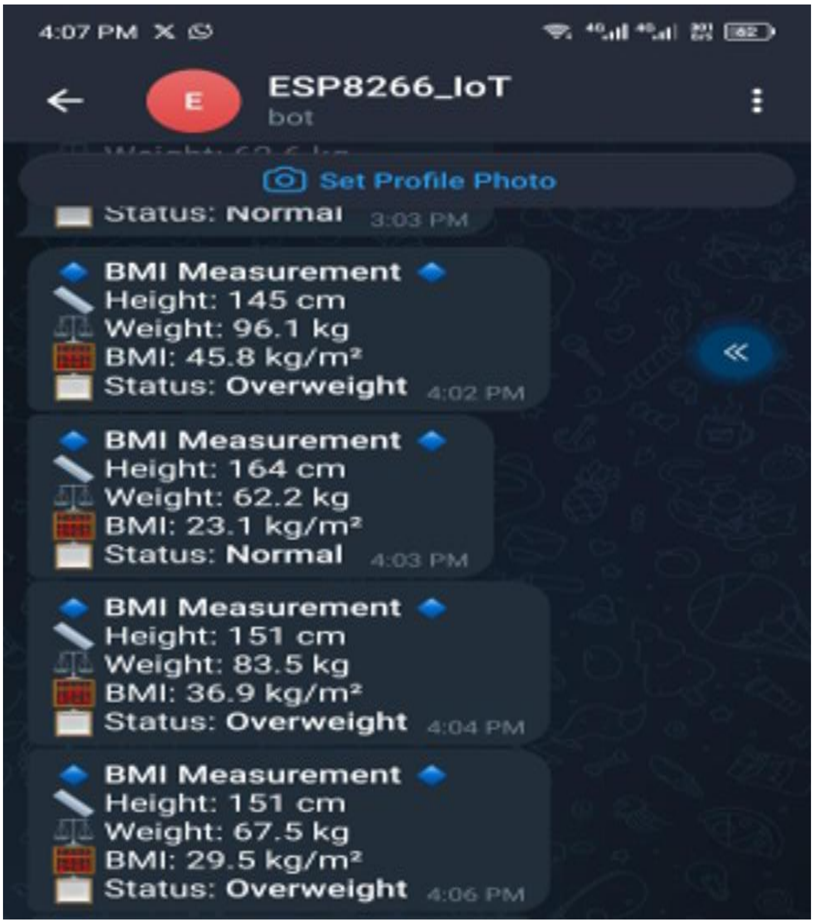

Figure 6. Pictures of results on the patient data based

The comparative empirical results obtained from testing one typical individual per World Health Organization (WHO) BMI categorization tier during the hardware calibration phase are shown in Table 1 below.

Table 1: Comparative Analysis of IoT-based Measurements device vs. Traditional Calibration Benchmarks

ID	Target Band	Trad. Height (cm)	IoT Height (cm)	Trad. Weight (kg)	IoT Weight (kg)	BMI (Traditional)	BMI (IoT)	Accuracy Variance
001	Under weight	172.0	172.5	51.3	52.1	17.33	17.48	**-0.15**
002	Normal	164.3	164.0	62.0	62.2	22.97	23.10	**-0.13**
003	Over weight	144.5	145.0	57.5	57.8	27.53	27.50	**-0.12**
004	Obese I	160.0	160.5	88.0	87.9	34.38	34.12	**-0.26**

ISSN No. 2454-6186 | DOI: 10.47772/IJRISS | Volume X Issue VI June 2026

005	Obese II	144.5	145.0	96.0	96.1	45.90	45.80	**-0.27**
006	Under weight	150.9	150.6	38.0	37.9	16.69	16.71	**-0.02**
007	Under weight	173.7	173.2	55.0	55.2	18.23	18.40	**-0.17**
008	Obese I	151.1	150.8	69.6	69.8	30.48	30.69	**-0.21**
009	Obese II	150.9	151.2	84.2	84.7	36.98	37.05	**-0.07**
010	Obese II	164.7	164.5	107.1	107.9	39.48	39.87	**-0.39**
011	Under weight	176.6	176.6	51.1	51.1	16.38	16.38	**0.00**
012	Over weight	155.4	155.2	71.9	71.7	29.77	29.77	**0.00**
013	Under weight	163.3	163.1	45.0	45.2	16.87	16.99	**-0.12**
014	Over weight	178.2	178.4	90.9	90.7	28.63	28.50	**0.13**
015	Obese I	152.8	153.1	73.5	73.7	31.48	31.44	**0.04**
016	Over weight	170.2	169.7	82.6	83.1	28.51	28.86	**-0.35**
017	Normal	177.1	177.6	78.1	78.0	24.90	24.73	**0.17**
018	Under weight	163.3	163.8	45.7	45.7	17.14	17.03	**0.11**
019	Normal	163.0	162.8	52.8	53.3	19.87	20.11	**-0.24**
020	Under weight	171.3	171.6	48.2	48.1	16.43	16.33	**0.10**
021	Normal	166.2	166.5	55.9	56.4	20.24	20.34	**-0.10**
022	Obese II	157.7	158.2	95.1	95.9	38.24	38.32	**-0.08**
023	Under weight	158.0	157.8	40.1	40.2	16.06	16.14	**-0.08**
024	Over weight	152.3	152.5	68.6	69.1	29.57	29.71	**-0.14**
025	Over weight	157.4	157.7	68.1	68.2	27.49	27.42	**0.07**
026	Normal	159.3	159.5	51.0	51.2	20.10	20.13	**-0.03**
027	Over weight	176.1	176.3	84.2	84.3	27.15	27.12	**0.03**
028	Over weight	157.7	157.9	74.6	74.7	30.00	29.96	**0.04**
029	Under weight	176.5	176.2	56.5	57.0	18.14	18.36	**-0.22**
030	Normal	177.7	177.2	67.1	67.2	21.25	21.40	**-0.15**
031	Obese I	170.9	170.7	94.5	94.7	32.36	32.50	**-0.14**
032	Under weight	173.8	174.0	49.2	50.0	16.29	16.51	**-0.22**
033	Over weight	176.9	176.7	83.6	83.7	26.71	26.81	**-0.10**
034	Normal	165.9	166.2	68.0	68.0	24.71	24.62	**0.09**
035	Obese II	176.7	176.2	125.1	125.9	40.07	40.55	**-0.48**
036	Over weight	179.5	179.2	88.7	88.6	27.53	27.59	**-0.06**
037	Over weight	176.7	177.2	86.5	86.7	27.70	27.61	**0.09**

038	Under weight	171.0	170.5	50.4	50.4	17.24	17.34	**-0.10**
039	Over weight	158.4	158.6	65.7	65.5	26.19	26.04	**0.15**
040	Under weight	175.6	176.1	55.6	55.8	18.03	17.99	**0.04**
041	Normal	154.5	154.7	51.5	51.4	21.57	21.48	**0.09**
042	Over weight	168.5	168.2	79.6	79.8	28.04	28.21	**-0.17**
043	Normal	175.0	175.3	64.6	65.1	21.09	21.18	**-0.09**
044	Over weight	165.3	164.8	75.4	75.3	27.59	27.73	**-0.14**
045	Normal	152.2	152.4	43.2	43.1	18.65	18.56	**0.09**
046	Obese II	157.7	158.0	88.8	88.6	35.71	35.49	**0.22**
047	Normal	152.4	152.2	43.4	43.2	18.69	18.65	**0.04**
048	Obese II	158.3	158.0	104.5	104.7	41.70	41.94	**-0.24**
049	Normal	175.3	175.5	74.5	74.6	24.24	24.22	**0.02**
050	Normal	177.5	177.2	74.8	74.6	23.74	23.76	**-0.02**
051	Under weight	173.1	173.1	50.6	50.7	16.89	16.92	**-0.03**
052	Under weight	173.6	173.1	55.6	55.4	18.45	18.49	**-0.04**
053	Obese I	175.5	175.0	104.7	104.6	33.99	34.16	**-0.17**
054	Normal	156.7	156.7	52.6	52.5	21.42	21.38	**0.04**
055	Over weight	166.2	165.7	81.1	81.2	29.36	29.57	**-0.21**

Sensor Accuracy and Variance

The experimental data show that there is very little margin of error between the automated IoT system and the manual clinical approaches.

Height Variance: The highest recorded height variance was ±0.5. The main causes of this variation are environmental echo scattering from nearby clothing and hair or slight changes in human posture during the ultrasonic sensor trigger delay.

Weight Variance: The weight error margin continuously stayed within ±0.2, confirming the accurate scale factor calibration of the HX711 amplifier.

Systemic Error: The cumulative BMI variance that resulted was between ±0.25 and ±0.27, meaning that the overall system accuracy rating was higher than 99.0%.

REFERENCES

1. Fadil, A., and Thamrin, M. (2020). Instrumentation Calibration Methods for Digital Load Cells in Clinical Engineering. *Journal of Robotics and Automation Engineering*, 22(1), pp. 89–97.
2. Faradisa, I. S., Muhammad, R. P., and Girindraswari, D. A. (2022). Design Body Mass Index (BMI) and Body Fat Percentage Using Fuzzy Logic. *Indonesian Journal of Electronics, Electromedical Engineering, and Medical Informatics*, *4*(2), 94–106. https://doi.org/10.35882/ijeeemi.v4i2.7
3. Hidayat, R., and Fajrianti, N. (2020). Automated Body Mass Index Calculation Using Arduino Architectures. *Journal of Medical Instrumentation*, 14(2), pp. 45–52.

ISSN No. 2454-6186 | DOI: 10.47772/IJRISS | Volume X Issue VI June 2026

4. Jilantikiri, L. J., Yahaya, S. A., Ajibola, T. M., Oluwajoba, A. S., and Obioha, C. A. (2022). Development of a Digital Body Mass Index (BMI) measuring device for low-resource settings. *Malawi Journal of Science and Technology*, *14*(1), 44–53.
5. Kaushal, S., Singh, S., and Sharma, A. (2020). A randomised study comparing the extent of block produced by spinal column height and body weight-based formulae for paediatric caudal analgesia. *Indian Journal of Anaesthesia*, *64*(6), 477–482. https://doi.org/10.4103/ija.IJA_824_19
6. Krisnadi, T., and Ridwanto, M. (2021). Smart Health Monitoring Kiosk Based on ESP8266 and Firebase Cloud Integration. *International Journal of Embedded Systems*, 8(3), pp. 112–119.
7. World Health Organization. (2021). *Body Mass Index - BMI Classification Guidelines*. WHO Technical Report Series.